





Magnetic Properties of 3d Metal Rods With Composition Gradients Produced by Electroless Deposition

Elena A. Denisova^{1,2} , Lidia A. Chekanova¹, Sergey V. Komogortsev^{1,3}, Svetlana A. Satsuk¹, Ivan V. Nemtsev^{1,2,4} , Rauf S. Iskhakov^{1,3} , and Sergey V. Semenov¹ 

¹Kirensky Institute of Physics, Federal Research Center KSC SB RAS, 660036 Krasnoyarsk, Russia

²Siberian Federal University, 660041 Krasnoyarsk, Russia

³Reshetnev Siberian State University of Science and Technology, 660037 Krasnoyarsk, Russia

⁴Krasnoyarsk Scientific Center, Federal Research Center KSC SB RAS, 660036 Krasnoyarsk, Russia

Received 13 Feb 2022, revised 18 Mar 2022, accepted 21 Mar 2022, published 29 Mar 2022, current version 5 May 2022.

Abstract—A comparative study of the magnetic properties of arrays of Co–Ni rods with different composition gradients (smooth or step-like) along the rod axes was carried out. Ordered arrays of Co–Ni nanorods with diameters up to 400 nm and 8 μm length were prepared by electroless plating into a porous nuclear-track-etched polycarbonate membrane. The gradient in Co and Ni composition was confirmed by energy-dispersive X-ray analysis. The variation of Co–Ni contents along the long axis of the rods correlates with the gradient of the magnetization within the rod. Magnetization reversal was studied by analyzing the angular dependence of coercivity and using micromagnetic simulations. For both types of gradient rods, reversal occurs by curling. The local magnetic anisotropy field of rods with a step-type gradient is significantly higher than that for rods with a smooth gradient.

Index Terms—Nanomagnetics, rods with gradients of composition, electroless deposition, coercivity, magnetic anisotropy.

I. INTRODUCTION

Structural and functional gradient materials, characterized by compositional or microstructural gradation along coordinate axes, make up a new class of advanced materials [Sudakar 2007]. Functionally graded materials (FGMs) are distinguished from isotropic materials by gradients of composition, phase distributions, porosity, texture, grain size, etc. Now FGMs are some of the most promising materials for microwave applications, for producing highly sensitive sensors, effective catalysts, for magnetic recording [Li 2008]. Nowadays, many researchers regard magnetization-graded ferromagnetic materials as magnetic counterparts of compositionally doped semiconductors [Mantese 2005].

Applied properties, such as coercivity and magnetic anisotropy, can be tailored by varying the shape, structure, and spatial distribution of magnetic functional units [Mendez 2017, Komogortsev 2019]. So, different types of geometrical and compositional modulations of magnetic nanowires (NWs) can be used to control functional magnetic characteristics for the fabrication of spintronic, magnetic data storage, and sensing devices [Parkin 2008, Darques 2009, Rial 2020]. To control the magnetization processes, NWs with modulations in diameter or material composition are being studied [Bran 2016, Wang 2018]. Magnetic multisegmented NWs or wires with step-like composition gradient are the focus of numerous works [Parkin 2008, Pereira 2015, Bran 2017, Garcia 2018, Wang 2019, Rial 2020]. However, a limited number of works have been reported on magnetic properties of NWs with smooth composition gradient [Zeng 2014, Aslam 2020].

The major applications of magnetic nanomaterials require an understanding of the magnetization reversal mechanisms. It is known that the different magnetization reversal mechanisms manifest a different angular dependence of the hysteresis loop [Han 2003, Tang 2006]. The reversal mode, and thus the nature of the domain wall, is determined by the wires' material and by the diameter and aspect ratio. Moreover, arrays of NWs have different magnetic properties than individual NWs. An array of NWs is characterized by an effective anisotropy. Both the shape anisotropy and magnetocrystalline anisotropy of individual NWs and the dipole–dipole interaction in the array contribute to the effective anisotropy of the array. The gradient distribution of magnetic Co and Ni elements along the NWs governs the structure of the NWs, which finally affect the magnetic properties [Yang 2016].

In this letter, we demonstrate the possibility to control functional magnetic characteristics of rods by means of composition architecture (smooth or step-like gradient). Here, we focused on static magnetic properties of Co–Ni rods with composition gradient. In this work, we have synthesized Co–Ni rods with large diameters up to 400 nm and lengths around 8 μm . The study of the magnetization reversal processes was performed by analyzing the angular dependence of coercivity and using micromagnetic simulations. Among the most important material characteristics are the values of anisotropy and saturation field. Magnetic anisotropy of composition-modulated materials in comparison with that for homogeneity in composition samples is the subject of this letter.

II. EXPERIMENTAL

The segmented Co–Ni rods (step-like composition gradient), Co–Ni alloy rods, and Co–Ni rods with gradient Ni content along the rod axis (smooth composition gradient) have been prepared by electroless

Corresponding author: Elena A. Denisova (e-mail: len-den@iph.krasn.ru). Trends in Magnetism Conference, Cefalù, Palermo, Italy, 6-10 September 2021. Digital Object Identifier 10.1109/LMAG.2022.3163015

plating of ferromagnetic metals into linear pores of nuclear track etched polycarbonate (PCTE) membrane with pore diameters 0.4 μm . One side of the membrane was coated by a thin layer of thermal-sputtered cooper. During deposition, the cooper layer was placed in contact with an aluminum foil to create an electrochemical potential [Ruscior 1971], and thus promote metal deposition into the pores of the PCTE membrane along the pore axis. It is known [Fert 1999] that Co and Ni have similar deposition potentials, so it is possible to carry out the co-deposition of Co and Ni from a single solution by electroless plating. The plating bath was comprised of source metal ion (CoSO_4 10 g/l) or (NiSO_4 15 g/l), complexing agent ($\text{Na}_3\text{C}_6\text{H}_5\text{O}_7$ 90 g/l), pH stabilizer [$(\text{NH}_4)_2\text{SO}_4$ buffer solution 40 g/l], and reducing agent (NaPO_2H_2 90 g/l). The pH value was adjusted by adding NH_4OH solution. The rods with gradient Co and Ni content along the rod axis were fabricated by gradually changing the pH value from 9 to 7 during the deposition process. The duration of depositions was 1 h. In the case of rods with the step-like composition gradient, samples were grown into PCTE membrane pores by electroless deposition using two different electrolytes: CoSO_4 (10 g/l) + $\text{Na}_3\text{C}_6\text{H}_5\text{O}_7$ (90 g/l) + $(\text{NH}_4)_2\text{SO}_4$ (40 g/l) + NaPO_2H_2 (90 g/l) and (NiSO_4 15 g/l) + $\text{Na}_3\text{C}_6\text{H}_5\text{O}_7$ (90 g/l) + $(\text{NH}_4)_2\text{SO}_4$ (40 g/l) + NaPO_2H_2 (90 g/l). Both segments were deposited at a constant pH (8.5) for different periods of time, 35 min for Ni and 25 min, respectively, for Co segments. The temperature of the solution was maintained with a thermostat at 85 $^\circ\text{C}$. It should be noted that a definite phosphorus admixture is always present in the resulting metal deposits because the reduction of hypophosphite to elemental phosphorus always occurs simultaneously with metal reduction.

The morphological characteristics and the elemental composition of the investigated materials were studied by scanning electron microscopy (S5500 and TM3000 Hitachi) and energy dispersive X-ray microanalysis (EDX). The crystalline structure of the rods was determined using a DRON-4 X-ray diffractometer operating with Cu K_α radiation. The magnetic hysteresis loops were measured using a vibrating sample magnetometer (VSM 8604 Lake Shore Cryotronics).

III. RESULTS AND DISCUSSION

A. Microstructural and Magnetic Characterization

Arrays of Co–Ni rods with diameters of ~ 400 nm, distances between rods varied in range from 0.2–1 μm , and aspect ratios (length/diameter) 10–20 were successfully obtained by electroless deposition inside linear pores of PCTE membranes. Scanning electron micrographs of the Co–Ni rods are shown in Fig. 1. The average length of rods is 8 μm . The EDX analysis data confirm the composition modulation in produced samples [see Fig. 1(c) and (d)]. For gradient rods, Co content changes practically linearly along the rod axis from 35 % to 75 %. According to the X-ray diffraction data, the Ni and Co alloys for the rods of all type (with even element distribution and gradient Ni content) were crystalline with an fcc structure.

To obtain data about macroscopic magnetic anisotropy of synthesized samples, we measure magnetization curves at different orientations of an external field. Figs. 2 and 3 show the hysteresis loop for the Co–Ni segmented rods and Co–Ni gradient rods. An angular dependence of the coercive field (H_c) in a cylinder of sufficiently large diameter ($D > \sqrt{A/M_s^2}$) is the result from the development of

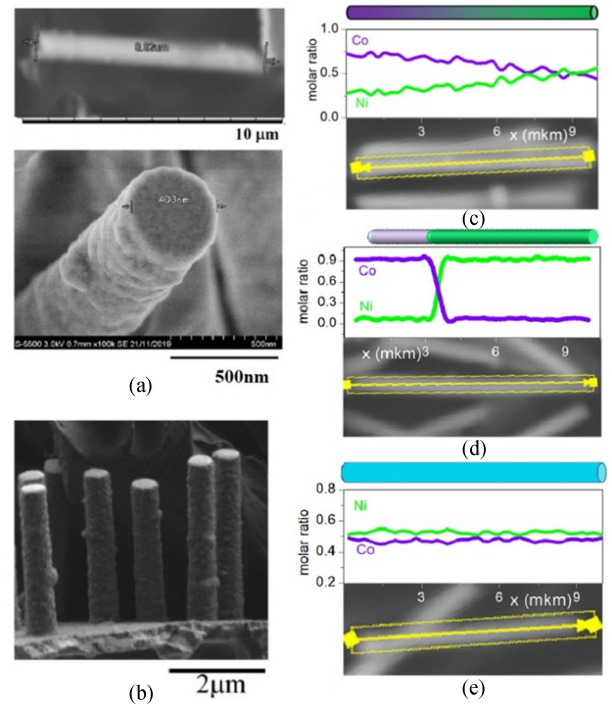


Fig. 1. SEM images of (a) the Co–Ni rod and (b) Co–Ni rods array, (c) EDX line-scan for Co–Ni gradient rod. (d) EDX line-scan for Co–Ni step-like rod. (e) EDX line-scan for Co–Ni rod with evenly element distribution.

magnetic state instability in the filament by the magnetization curling [Aharoni 1997]. According to Aharoni [1997] for H_c that is equal to the instability field

$$H_c = \frac{H_d ab}{\sqrt{a^2 \sin^2(\varphi) + b^2 \cos^2(\varphi)}} \quad (1)$$

where $H_d = 2\pi M_s$, $a = 2N_z - 1.08(l_0/D)^2$, $2b = 2N_x - 1.08(l_0/D)^2$, $l_0 = \sqrt{A/M_s^2}$, N_z , N_x — demagnetizing factors along and across filament. The solid lines in Figs. 3(b) and 4(b) are calculated according to (1), considering the sizes of the cylinder and constants $A = 1 \cdot 10^{-6}$ erg/cm, $M_s = 1000$ G, as well as a decrease in the effective demagnetizing factor N_z associated with the interaction in the filament ensemble [Denisova 2022]. The dipole–dipole interaction between wires results in $H_d = 2\pi M_s (1-3P)$, where P is the membrane porosity (in our case $P \approx 6\%$). Note, however, that good agreement between the calculated and experimental data can be achieved for fitting parameter $H_d = 56 \pm 1$ Oe for the case of rods with the step-like composition profile and $H_d = 59 \pm 1$ Oe for the rods with the smooth composition profile that are both much less than $2\pi M_s$. The reason of such a decrease can be the polycrystalline structure of the filament, as well as misorientation in the filament system, leading to the remanent magnetization much less than M_s even along the easiest magnetization axis.

The low eccentricity of the ellipse $H_c(\varphi)$ for the rods with a sharp compositional gradient in comparison with $H_c(\varphi)$ for the rods with the smooth composition profile is clear within the analysis by (1). The fact is that with a constant length of filaments set by the thickness of the membrane, the aspect ratio of the magnetic cylindrical segments is lower, which inevitably leads to a decrease in the difference between the parameters a and b in (1).

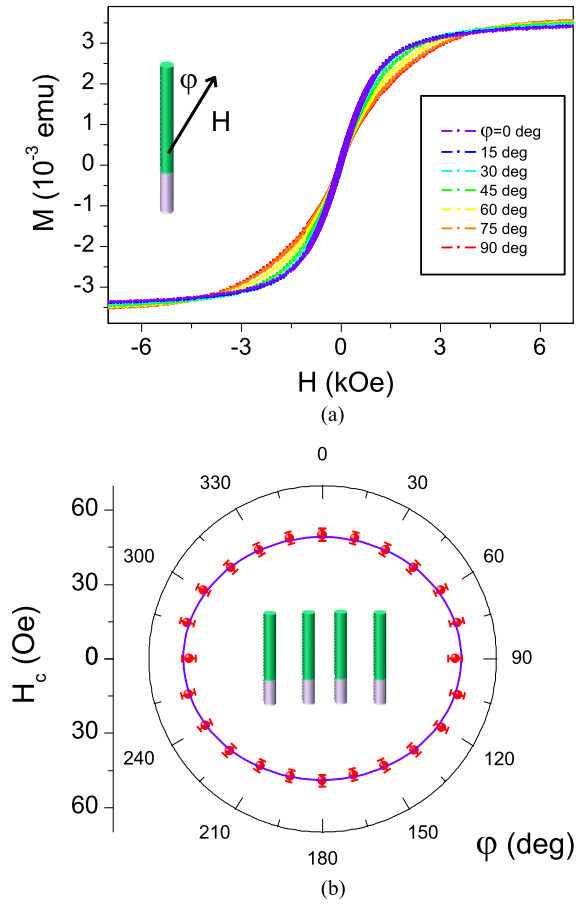


Fig. 2. (a) Magnetization curves and (b) coercivity H_c for Co–Ni rods with the step-like composition profile. The solid line in Fig. 2(b) is drawn according to (1) with $H_d = 56 \pm 1$ Oe, a and b parameters calculated using rod sizes and magnetic constants (see text). In the scheme, the green part corresponds to the Ni segment.

B. Micromagnetic Simulation

Micromagnetic modeling of the rods was carried out in order to reveal the influence of the magnetization gradient, as well as the rod nanostructure on the magnetic properties. The simulation was performed using the OOMMF package [Donahue 1999]. In the micromagnetic simulations, the values for the variables that we use are very similar to the ones reported in Talagala [2002]: the exchange interaction constant $A = 1 \cdot 10^{-6}$ erg/cm, the size of the cubic cell in the finite difference method $5 \text{ nm} \times 5 \text{ nm} \times 5 \text{ nm}$, and the magnetization $M_s = 1000$ G (for a uniform rod), and for a gradient rod, linear changing along the filament from 500 to 1000 G is set. Previously, the linear behavior of magnetization with Ni content in NiCo alloy was experimentally established [Hinoul 1972]. Since the rods we are dealing with in the experiment are polycrystalline, we also considered the polycrystalline structure of the rod in the simulation. One crystallite contained of 64 cells (crystallite size 20 nm). The square cross section of the rod contained 2×2 crystallites, and the 100 crystallites were along length. The direction of the easy magnetization axis (EMA) of the cells within one crystallite was set uniformly, whereas in the system of crystallites, the EMAs were oriented randomly with the anisotropy constant ($5 \cdot 10^4$ erg/cm³).

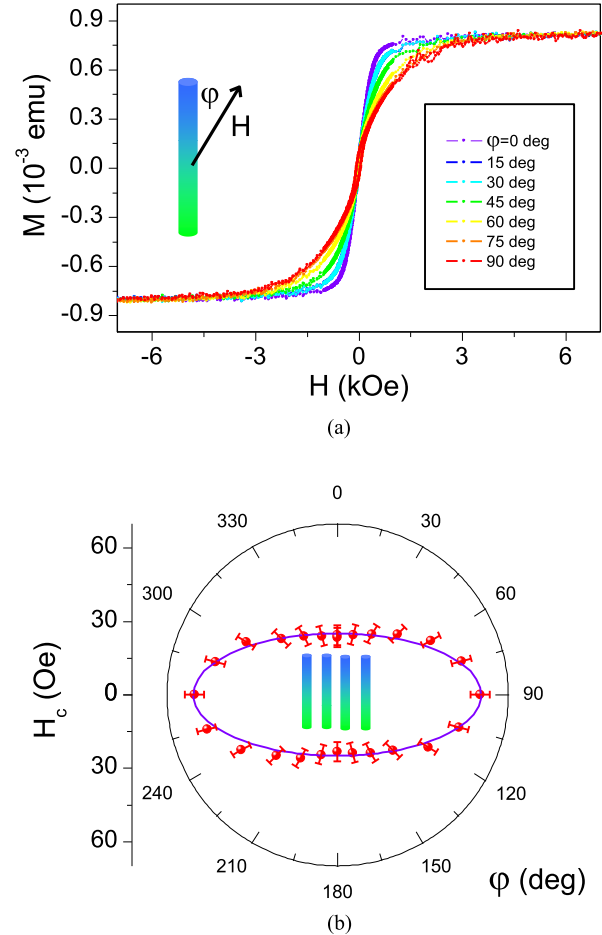


Fig. 3. (a) Magnetization curves and (b) coercivity H_c for Co–Ni rods with the smooth composition profile. The solid line in Fig. 3(b) is drawn according to (1) with $H_d = 59 \pm 1$ Oe.

The numerical results in Fig. 4 are compared with the calculations using (1). It turns out that if we use $H_d = 2\pi M_s$ in (1), the values of H_c significantly exceed the results of the numerical experiment (outer ellipse in Fig. 5). To achieve agreement with the numerical data (solid line closed to the symbols), we used the value $H_d = 0.36 \times 2\pi M_s$. This value is almost three times less than H_d for a homogeneous rod due to the polycrystalline structure of the filament [Satsuk 2021]. For the angles close to 90° , the coercive field is no longer determined by the instability field described by (1), but approaches zero at 90° .

In the experiment, this behavior is not observed, which may be due to 1) a certain random deviation of the filaments in the membrane from the vertical and 2) with a larger value of the local anisotropy constant than that used for calculations. To obtain information about the local magnetic anisotropy in rods obtained by chemical deposition, below we study them using the approach to magnetic saturation technique. Note that in Fig. 4, the angular dependence of a uniform rod is in qualitative agreement with (1) for angles far from 90° . For a rod with a magnetization gradient, noticeable deviations from (1) are observed, whereas the value of the reduced H_c for angles close to 0° is noticeably higher than that for a homogeneous rod. The magnetization reversal (see Fig. 4) occurs by both curling (at $0^\circ \div 70^\circ$ and (1) is acceptable of course for this range of angles only) and coherent reversal (or transverse domain wall propagation at $70^\circ \div 90^\circ$). This behavior is similar to that reported for magnetic NWs and nanotubes [Escrig 2008].

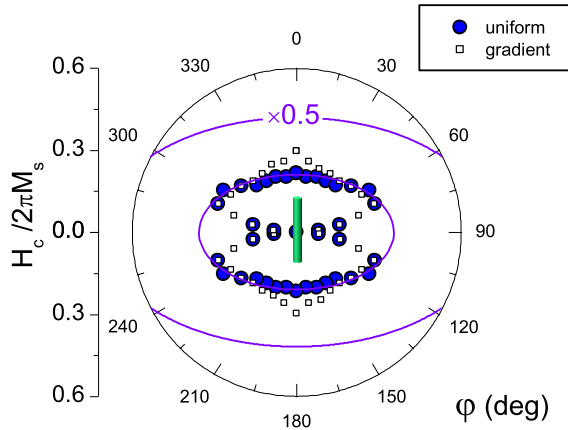


Fig. 4. Simulated angular dependences of a uniform nanorod (round symbols) and a rod with the linear magnetization gradient (square symbols). Lines correspond the calculation according to (1). The line close to the symbols is for the value $H_d = 0.36 \times 2\pi M_s$, and the outer ellipse is for $H_d = 2\pi M_s$.

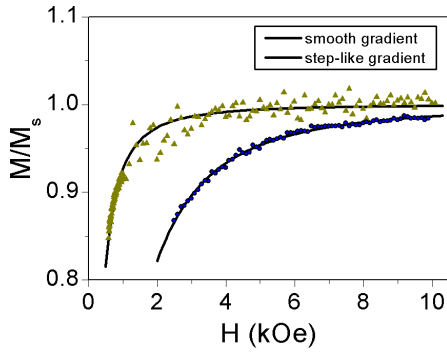


Fig. 5. Magnetization deviation from saturation for the rods with smooth gradient (green triangles) and rod with step-like composition gradient (blue circle). The black lines represent the respective fittings using (2).

C. Local Magnetic Anisotropy Field

The local magnetic anisotropy field is studied using the approach to magnetic saturation technique [Komogortsev 2017]. Fig. 5 shows typical magnetization curves for Co–Ni rods with different composition gradient. We fit the experimental approach to magnetic saturation curves with the following equation [Komogortsev 2017]:

$$\frac{\Delta M}{M_s} = \frac{(aH_a)^2}{H^{\frac{4-d}{2}} (H^{d/2} + H_R^{d/2})}. \quad (2)$$

Here, $M_a = 2K/M_s$ is a local magnetic anisotropy field, K is the magnetic anisotropy energy constant, a is a coefficient equal to $1/15^{1/2}$ for uniaxial anisotropy, and $(2/105)^{0.5}$ for cubic anisotropy, $H_R = 2A/(M_s R_c^2)$ is an exchange field, R_c is a correlation length of local EMA, d is the spatial dimension of nanograin distribution. M_a contains contributions of magnetocrystalline anisotropy and anisotropy induced by internal stresses. The good quality of fitting by (2) in Fig. 5 indicates the applicability of the theory of random magnetic anisotropy. According to this theory, the approach to magnetic saturation is determined by the local magnetic anisotropy and by the dimension of the anisotropy inhomogeneities. These parameters in (2) are determined as fitting parameters and are given in Table 1.

TABLE 1. Magnetic characteristics for Co–Ni rods with different element distribution.

	aH_a , kOe	d	H_R , kOe
rod: smooth composition gradient	0.42	2	1.5
rod: step-like composition gradient	1.21	3	2.1
film: smooth composition gradient	0.25	3	0.8

As you can see, the local magnetic anisotropy field for films is smaller than those for rods with the same type of composition gradient. The impact of the shape of the ferromagnetic materials on their local magnetic anisotropy may be attributed to the influence of surface layer or curvature. The existence of an additional interface boundary causes an increase in the anisotropy field for all samples.

IV. CONCLUSION

The magnetic properties of compositionally modulated Co–Ni nanorods with smooth and step-like composition profiles along the rod have been studied. Nanorods were prepared in the pores of polycarbonate membrane by electroless deposition. The composition gradient sets the gradient of the magnetization within the rod. Macroscopic magnetic anisotropy for an ensemble of rods in membranes with the same rod packing density is different: for rods with a smooth gradient, this anisotropy is higher than for rods with a stepped gradient. Magnetization reversal is carried out by the curling mechanism. Micromagnetic modeling performed considering the polycrystalline structure of the filament shows that the magnetization gradient affects both the magnitude of the coercive force and its angular dependence. Some discrepancy between experiment and simulation is apparently explained by imperfect orientation of the rods in the membrane and dipole–dipole interaction in the system of rods. Since the simulation showed the importance of taking into account the magnetic anisotropy of individual crystallites, the latter was experimentally studied using an approach to magnetic saturation. It turned out that the local magnetic anisotropy field in rods with a step-type gradient is significantly higher than in rods with a smooth gradient. In addition, the rods of two types exhibit magnetic anisotropy inhomogeneity of different shapes. The difference in magnetic properties in rods with a compositional gradient of different types indicates the possibility of tuning their properties by controlling the profile and magnitude of the rod magnetization gradient.

ACKNOWLEDGMENT

This work was supported in part by the Russian Foundation for Basic Research (RFBR), Krasnoyarsk Territory and in part by the Krasnoyarsk Regional Fund of Science under Grant 20-43-240003. The authors thank the Center of Collective Use of the Federal Research Center Krasnoyarsk Science Center of the Siberian Branch of the Russian Academy of Sciences for the equipment. Sergey V. Komogortsev thank the RFBR, Krasnoyarsk Region and the Krasnoyarsk Regional Science Foundation (Project 20-42-240001) for the support in the contribution of numerical simulation. The authors also thank V. S. Plotnikov and V. V. Tkachev for electron microscopy images.

REFERENCES

- Aharoni A (1997), "Angular dependence of nucleation by curling in a prolate spheroid," *J. Appl. Phys.*, vol. 82, pp. 1281–1287, doi: [10.1063/1.365899](https://doi.org/10.1063/1.365899).
- Aslam S, Das A, Khanna M, Kuanr B K (2020), "Concentration gradient Co–Fe nanowire arrays: Microstructure to magnetic characterizations," *J. Alloy Compd.*, vol. 838, 155566, doi: [10.1016/j.jallcom.2020.155566](https://doi.org/10.1016/j.jallcom.2020.155566).
- Bran C, Berganza E, Palmero E M, Fernandez-Roldan J A, Del Real R P, Aballe L, Foerster M, Asenjo A, Fraile Rodríguez A, Vázquez M (2016), "Spin configuration of cylindrical bamboo-like magnetic nanowires," *J. Mater. Chem. C*, vol. 4, pp. 978–984, doi: [10.1039/C5TC04194E](https://doi.org/10.1039/C5TC04194E).
- Bran C, Ivanov Y P, Kosel J, Chubykalo-Fesenko O, Vázquez M (2017), "Co/Au multisegmented nanowires: A 3D array of magnetostatically coupled nanopillars," *Nanotechnology*, vol. 28, 095709, doi: [10.1088/1361-6528/aa585f](https://doi.org/10.1088/1361-6528/aa585f).
- Darques M, Spiegel J, De la Torre Medina J, Huynen I, Piroux L (2009), "Ferromagnetic nanowire-loaded membranes for microwave electronics," *J. Magn. Magn. Mater.*, vol. 321, pp. 2055–2065, doi: [10.1016/j.jmmm.2008.03.060](https://doi.org/10.1016/j.jmmm.2008.03.060).
- Denisova E A, Chekanova L A, Komogortsev S V, Rautsky M V, Nemtsev I V, Iskhakov R S, Plotnikov V S, Tkachev V V, Li O A, Dolgoplova M V (2022), "Core-shell and bi-segmented cobalt-nickel nanorods prepared by electroless deposition," *IEEE Trans. Magn.*, vol. 58, 2300805, doi: [10.1109/TMAG.2021.3098747](https://doi.org/10.1109/TMAG.2021.3098747).
- Donahue M J, Porter D G (1999), *OOMMF User's Guide, Version 1.0*. Nat. Inst. Standards Technol., Gaithersburg, MD, USA. [Online]. Available: https://math.nist.gov/oommf/doc/userguide12b4/userguide/Overview_OOMMF.html
- Dryden D M, Sun T, McCormick R, Hickey R, Vidu R, Stroeve P (2016), "Anomalous deposition of Co–Ni alloys in film and nanowire morphologies from citrate baths," *Electrochimica Acta*, vol. 220, pp. 595–600, doi: [10.1016/j.electacta.2016.10.073](https://doi.org/10.1016/j.electacta.2016.10.073).
- Escrig J, Bachmann J, Jing J, Daub M, Altbir D, Nielsch K (2008), "Crossover between two different magnetization reversal modes in arrays of iron oxide nanotubes," *Phys. Rev. B*, vol. 77, 214421, doi: [10.1103/PhysRevB.77.214421](https://doi.org/10.1103/PhysRevB.77.214421).
- Fernández J G, Martínez V V, Thomas A, De la Prida Pidal V M, Nielsch K (2018), "Two-step magnetization reversal FORC fingerprint of coupled bi-segmented Ni/Co magnetic nanowire arrays," *Nanomaterials*, vol. 8, 548, doi: [10.3390/nano8070548](https://doi.org/10.3390/nano8070548).
- Fert A, Piroux L (1999), "Magnetic nanowires," *J. Magn. Magn. Mater.*, vol. 200, pp. 338–358, doi: [10.1016/S0304-8853\(99\)00375-3](https://doi.org/10.1016/S0304-8853(99)00375-3).
- Han G C, Zong B Y, Luo P, Wu Y H (2003), "Angular dependence of the coercivity and remanence of ferromagnetic nanowire arrays," *J. Appl. Phys.*, vol. 93, pp. 9202–9207, doi: [10.1063/1.1572197](https://doi.org/10.1063/1.1572197).
- Hinoul M, Witters J (1972), "Exchange constants in nickel-cobalt alloys from standing spin wave resonance," *Solid State Commun.*, vol. 10, pp. 749–752, doi: [10.1016/0038-1098\(72\)90185-8](https://doi.org/10.1016/0038-1098(72)90185-8).
- Komogortsev S V, Chekanova L A, Denisova E A, Bukaemskiy A A, Iskhakov R S, Mel'nikova S V (2019), "Macro- and nanoscale magnetic anisotropy of FeNi(P) micropillars in polycarbonate membrane," *J. Supercond. Novel Magn.*, vol. 32, pp. 911–916, doi: [10.1007/s10948-018-4772-y](https://doi.org/10.1007/s10948-018-4772-y).
- Komogortsev S V, Iskhakov R S (2017), "Law of approach to magnetic saturation in nanocrystalline and amorphous ferromagnets with improved transition behavior between power-law regimes," *J. Magn. Magn. Mater.*, vol. 440, pp. 213–216, doi: [10.1016/j.jmmm.2016.12.145](https://doi.org/10.1016/j.jmmm.2016.12.145).
- Li S, Huang Z, Duh J-G, Yamaguchi M (2008), "Ultrahigh-frequency ferromagnetic properties of FeCoHf films deposited by gradient sputtering," *Appl. Phys. Lett.*, vol. 92, 092501, doi: [10.1063/1.2889447](https://doi.org/10.1063/1.2889447).
- Mantese J V, Micheli A L, Schubring N W, Hayes R W, Srinivasan G, Alpay S P (2005), "Magnetization-graded ferromagnets: The magnetic analogs of semiconductor junction elements," *Appl. Phys. Lett.*, vol. 87, 082503, doi: [10.1063/1.2012526](https://doi.org/10.1063/1.2012526).
- Méndez M, González S, Vega V, Teixeira J M, Hernando B, Luna C, Prida V M (2017), "Ni-Co alloy and multisegmented Ni/Co nanowire arrays modulated in composition: Structural characterization and magnetic properties," *Crystals*, vol. 7, 66, doi: [10.3390/cryst7030066](https://doi.org/10.3390/cryst7030066).
- Parkin S S, Hayashi M, Thomas L (2008), "Magnetic domain-wall racetrack memory," *Science*, vol. 320, pp. 190–194, doi: [10.1126/science.1145799](https://doi.org/10.1126/science.1145799).
- Pereira A, Palma J L, Vázquez M, Denardin J C, Escrig J (2015), "A soft/hard magnetic nanostructure based on multisegmented CoNi nanowires," *Phys. Chem. Chem. Phys.*, vol. 17, pp. 5033–5038, doi: [10.1039/C4CP05665E](https://doi.org/10.1039/C4CP05665E).
- Rial J, Proenca M P (2020), "A novel design of a 3D racetrack memory based on functional segments in cylindrical nanowire arrays," *Nanomaterials*, vol. 10, 2403, doi: [10.3390/nano10122403](https://doi.org/10.3390/nano10122403).
- Ruscior C, Croial E (1971), "Chemical iron-phosphorus films," *J. Electrochem. Soc.*, vol. 118, pp. 696–698, doi: [10.1149/1.2408146](https://doi.org/10.1149/1.2408146).
- Satsuk S A, Komogortsev S V (2021), "Micromagnetic modeling of the polycrystalline structure effect to the hysteresis loop in ferromagnetic nanowire," *J. Phys.: Conf. Ser.*, vol. 1847, 012045, doi: [10.1088/1742-6596/1847/1/012045](https://doi.org/10.1088/1742-6596/1847/1/012045).
- Sudakar C, Naik R, Lawes G (2007), "Internal magnetostatic potentials of magnetization-graded ferromagnetic materials," *Appl. Phys. Lett.*, vol. 90, 062502, doi: [10.1063/1.2437721](https://doi.org/10.1063/1.2437721).
- Talagala P, Fodor P S, Haddad D, Naik R, Wenger L E, Vaishnav P P, Naik V M (2002), "Determination of magnetic exchange stiffness and surface anisotropy constants in epitaxial Ni_{1-x}Co_x(001) films," *Phys. Rev. B*, vol. 66, 144426, doi: [10.1103/PhysRevB.66.144426](https://doi.org/10.1103/PhysRevB.66.144426).
- Tang X-T, Wang G-C, Shima M (2006), "Field angle and thickness dependence of coercivity in electrodeposited CoNi–Cu multilayer nanowires," *IEEE Trans. Magn.*, vol. 42, pp. 2975–2977, doi: [10.1109/TMAG.2006.878399](https://doi.org/10.1109/TMAG.2006.878399).
- Wang D-S, Mukhtar A, Wu K-M, Gu L, Cao X (2019), "Multi-segmented nanowires: A high tech bright future," *Materials*, vol. 12, 3908, doi: [10.3390/ma12233908](https://doi.org/10.3390/ma12233908).
- Wang J, Zuo Z, Huang L, Warsi M A, Xiao J Q, Hu J (2018), "Novel gradient-diameter magnetic nanowire arrays with unconventional magnetic anisotropy behaviors," *Chem. Commun.*, vol. 54, pp. 7515–7518, doi: [10.1039/C8CC02294A](https://doi.org/10.1039/C8CC02294A).
- Yang H, Li Y, Zeng M, Cao W, Bailey W E, Yu R (2016), "Static and dynamic magnetization of gradient FeNi alloy nanowire," *Sci. Rep.*, vol. 6, 20427, doi: [10.1038/srep20427](https://doi.org/10.1038/srep20427).
- Zeng M, Yang H, Liu J, Yu R (2014), "Gradient magnetic binary alloy nanowire," *J. Appl. Phys.*, vol. 115, 17B514, doi: [10.1063/1.4864248](https://doi.org/10.1063/1.4864248).